Mon. Not. R. Astron. Soc. **000**, 1–?? (2011) Printed 4 May 2012 (MN LaTeX style file v2.2)

# Detection of gravity modes in the massive binary V380 Cyg from *Kepler* spacebased photometry and high-resolution spectroscopy⋆

A. Tkachenko,[1] C. Aerts,[1,2,3] K. Pavlovski,[4] J. Southworth,[5] P. Degroote,[1] J. Debosscher,[1] M. Still,[6] S. Bryson,[6] G. Molenberghs,[3] S. Bloemen,[1] B. L. de Vries,[1] M. Hrudkova,[7,8] R. Lombaert,[1] P. Neyskens,[9] P. I. Pápics,[3] G. Raskin,[1] H. Van Winckel,[1] R. L. Morris,[10] D. T. Sanderfer,[11] and S. E. Seader[10]

[1]*Instituut voor Sterrenkunde, KU Leuven, Celestijnenlaan 200D, B-3001 Leuven, Belgium*
[2]*Department of Astrophysics, IMAPP, Radboud University Nijmegen, 6500 GL Nijmegen, The Netherlands*
[3]*Center for Statistics (CenStat), University of Hasselt, Agoralaan 1, B-3590 Diepenbeek, Belgium*
[4]*Department of Physics, University of Zagreb, Bijenička cesta 32, 10000 Zagreb, Croatia*
[5]*Astrophysics Group, Keele University, Staffordshire ST5 5BG, UK*
[6]*NASA Ames Research Center/Bay Area Environmental Research Institute, MS 244-30, Moffett Field, CA 94 035, USA*
[7]*Thüringer Landessternwarte Tautenburg, 07778 Tautenburg, Germany*
[8]*Isaac Newton Group of Telescopes, Apartado de Correos 321, E-387 00 Santa Cruz de la Palma, Canary Islands, Spain*
[9] *Institut d'Astronomie et d'Astrophysique, Université Libre de Bruxelles, CP 226 Brussels, Belgium*
[10] *SETI Institute/NASA Ames Research Center, Moffett Field, CA 94035*
[11]*NASA Ames Research Center, Moffett Field, CA 94035*



Received date; accepted date

**ABSTRACT**

We report the discovery of low-amplitude gravity-mode oscillations in the massive binary star V380 Cyg, from 180 d of *Kepler* custom-aperture space photometry and 5 months of high-resolution high signal-to-noise spectroscopy. The new data are of unprecedented quality and allowed to improve the orbital and fundamental parameters for this binary. The orbital solution was subtracted from the photometric data and led to the detection of periodic intrinsic variability with frequencies of which some are multiples of the orbital frequency and others are not. Spectral disentangling allowed the detection of line-profile variability in the primary. With our discovery of intrinsic variability interpreted as gravity mode oscillations, V380 Cyg becomes an important laboratory for future seismic tuning of the near-core physics in massive B-type stars.

**Key words:** binaries: eclipsing — stars: individual (V380 Cyg) — stars: fundamental parameters — stars: variables: general — stars: oscillations

## 1 INTRODUCTION

V380 Cyg (HD 187879, KIC 5385723) is a bright ($V$ = 5.68) double-lined detached eclipsing binary with two early-B type components in a 12.426 d eccentric ($e$ = 0.23) orbit. It is an important test for massive star models, with a primary star about to start the hydrogen shell burning phase and a secondary still in the early part of the main sequence. V380 Cyg has been the subject of numerous studies, of which Popper & Guinan (1998), Guinan et al. (2000), and Pavlovski et al. (2009) are the most extensive, to which we refer for details on the properties of the system.

The interpretation of the stellar parameters of V380 Cyg deduced from the binary data is problematic in the sense that an extreme core overshooting parameter value above 0.5 (in local pressure scale heights) is needed to match them to theoretical evolutionary tracks (Pavlovski et al. 2009). Such a high core overshooting is not supported by recent seismic estimates, which rather point to values below 0.2 for single B-type pulsators with similar masses (e.g., Aerts et al. 2003, 2011; Pamyatnykh et al. 2004; Briquet et al. 2011). Nevertheless, Briquet et al. (2007) deduced an overshooting parameter of $0.44 \pm 0.07$ for the $8.2 \pm 0.3\,M_\odot$ primary of the detached spectroscopic binary $\theta$ Oph.

⋆ Based on DDT data gathered with NASA's Discovery mission *Kepler* and with the HERMES spectrograph, installed at the Mercator Telescope, operated on the island of La Palma by the Flemish Community, at the Spanish Observatorio del Roque de los Muchachos of the Instituto de Astrofísica de Canarias and supported by the Fund for Scientific Research of Flanders (FWO), Belgium, the Research Council of K.U.Leuven, Belgium, the Fonds National de la Recherche Scientific (F.R.S.–FNRS), Belgium, the Royal Observatory of Belgium, the Observatoire de Genève, Switzerland and the Thüringer Landessternwarte Tautenburg, Germany.

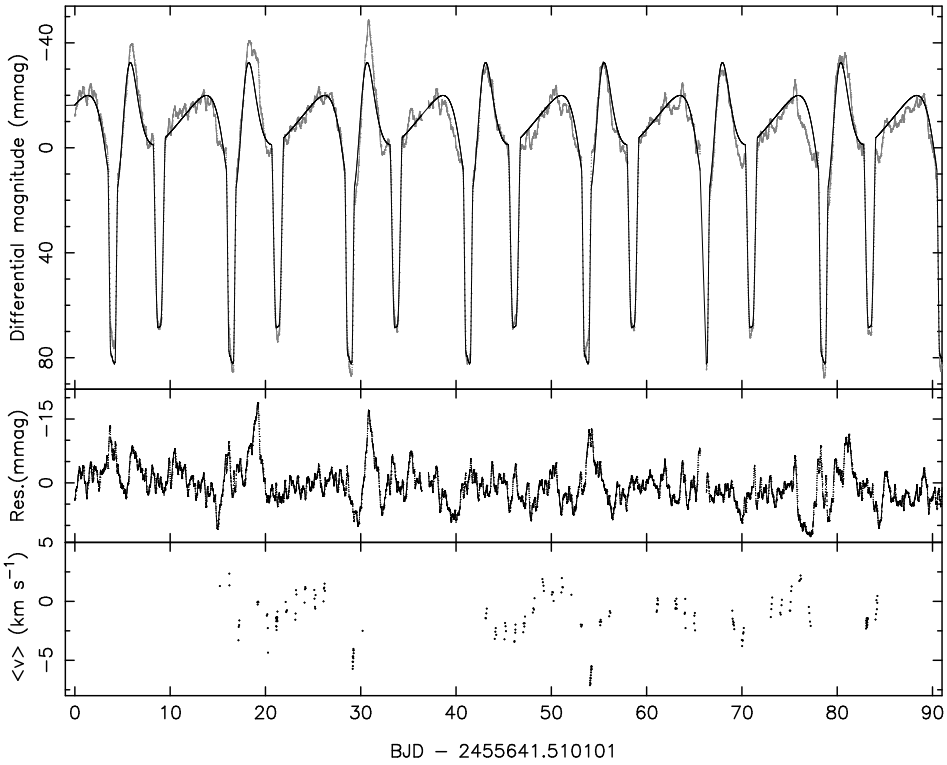


**Figure 1.** Upper panel: *Kepler* light curve of V380 Cyg observed during Q9 (gray) with the binary model overplotted (black). Middle panel: residual light curve. Lower panel: first moment of the disentangled Si III line of the primary.

Clearly, an independent seismic evaluation of the core overshooting parameter of the components of V380 Cyg is of major importance. However, despite the position of the two binary components in the instability strips for B stars, searches for oscillations in the binary so far led to null detections. We report the discovery of intrinsic variability from uninterrupted high-precision space photometry obtained by the *Kepler* satellite and interpret it in terms of gravity (*g*-mode) oscillations of the primary.

## 2 OBSERVATIONS

### 2.1 *Kepler* customized aperture photometry

The case study of the prototypical pulsator RR Lyr, with a maximum brightness of $V = 7.06$ during its pulsation cycle, showed that *Kepler*'s instrument is capable of performing high-precision photometry on saturated targets (Bryson et al. 2010; Kolenberg et al. 2011) by using a customized aperture mask. A dedicated mask was thus defined to collect all flux from V380 Cyg and the binary was successfully observed in short cadence (58 s) mode during Quarter 7 (Q7) of the mission, for about 90 d continuously. This led to the conclusion that low-amplitude variability occurs, aside variability from the eclipses and brightenings, so the star was reobserved during Quarter 9 (Q9).

The Q9 *Kepler* light curve is shown in Fig. 1. Variability on timescales shorter than the orbital period is obvious throughout the entire dataset, including during the eclipses. The *Kepler* light curve is fully compatible with but more precise than ground-based photometric data, which had previously revealed scatter at the mmag level (Guinan et al. 2000).

### 2.2 HERMES high-resolution spectroscopy

Given the discovery of low-amplitude variability in the *Kepler* Q7 data, we initiated a ground-based spectroscopic campaign. We acquired an extensive time-series of high-resolution, high signal-to-noise (S/N) spectra, starting during *Kepler* Q9 and lasting for 142 days. The spectra were taken with HERMES, the fibre-fed high-resolution spectrograph on the Mercator telescope (Observatorio del Roque de los Muchachos, La Palma, Canary Islands), which samples the entire optical range (380–900 nm) with a resolution of 85 000 (Raskin et al. 2011). We obtained 150 observations during out-of-eclipse phases and 256 exposures during primary or secondary eclipses. The typical exposure time was 1200 s. The data taken simultaneously with the *Kepler* Q9 observations is represented on Fig. 1.

The reduction of the spectra has been carried out using the dedicated HERMES software pipeline, including bias subtraction, cosmic ray filtering, flat fielding, wavelength calibration using a ThAr lamp, and order merging. Normalization to the local continuum was done manually by fitting a spline function to carefully selected continuum points. We computed Least Squares Deconvolution (LSD) profiles following Donati et al. (1997). These are shown in a gray-scale representation according to the orbital period of $P_{\rm orb} = 12.425719$ d (Guinan et al. 2000) in Fig. 2. The double-lined nature of the binary is clearly recovered in our high-quality spectroscopy.

**Table 1.** Summary of the parameters for the WD2004 solution of the *Kepler* short-cadence light curve of V380 Cyg. For further details on the control parameters we refer to the WD2004 user guide (Wilson & Van Hamme 2004). A and B refer to the primary and secondary stars, respectively.

| Parameter | WD2004 name | Value(±Error) |
|---|---|---|
| *Control parameters:* | | |
| WD2004 operation mode | MODE | 0 |
| Treatment of reflection | MREF | 2 (detailed) |
| Number of reflections | NREF | 2 |
| Limb darkening law | LD | 1 (linear) |
| Numerical grid size (normal) | N1, N2 | 60 |
| Numerical grid size (coarse) | N1L, N2L | 40 |
| *Fixed parameters:* | | |
| Orbital period ($P_{\rm orb}$, d) | PERIOD | 12.425719 |
| Reference time of minimum (BJD) | HJD0 | 2441256.544 |
| Mass ratio ($q$) | RM | 0.62 |
| Effective temperature A ($T_{\rm eff}^{\rm A}$, K) | TAVH, TAVC | 21500 |
| Effective temperature B ($T_{\rm eff}^{\rm B}$, K) | TAVH, TAVC | 22000 |
| Rotation rates | F1, F2 | 1.0 |
| Gravity darkening | GR1, GR2 | 1.0 |
| Bolometric albedos | ALB1, ALB2 | 1.0 |
| Bolometric LD coeff. A | XBOL1 | 0.648 |
| Bolometric LD coeff. B | XBOL2 | 0.685 |
| Third light | EL3 | 0.0 |
| Passband LD coeff. B | X2 | 0.262 |
| *Fitted parameters:* | | |
| Phase shift | PSHIFT | -0.0493±0.0003 |
| Star A potential | PHSV | 4.62±0.05 |
| Star B potential | PHSV | 11.1±0.6 |
| Orbital inclination ($i$, °) | XINCL | 80.5±0.5 |
| Orbital eccentricity ($e$) | E | 0.235±0.005 |
| Longitude of periastron ($\omega$, °) | PERR0 | 135±2 |
| Light from star A | HLUM | 12.02±0.10 |
| Light from star B | CLUM | 0.777±0.011 |
| Passband LD coeff. A | X2 | 0.08±0.03 |
| *Derived parameters:* | | |
| Fractional radius of star A ($R_{\rm A}/a$) | | 0.2655±0.0020 |
| Fractional radius of star B ($R_{\rm B}/a$) | | 0.0648±0.0011 |
| *Physical properties:* | | |
| Mass of star A ($M_{\rm A}$, $M_\odot$) | | 11.80±0.13 |
| Mass of star B ($M_{\rm A}$, $M_\odot$) | | 7.194±0.055 |
| Radius of star A ($R_{\rm A}$, $R_\odot$) | | 16.00±0.13 |
| Radius of star B ($R_{\rm B}$, $R_\odot$) | | 3.904±0.067 |
| Surface gravity star A (log$g$) | | 3.102±0.007 |
| Surface gravity star B (log$g$) | | 4.112±0.015 |
| Orbital semimajor axis ($a$, $R_\odot$) | | 60.25±0.19 |
| $\log(L_{\rm A}/L_\odot)$ | | 4.711±0.023 |
| $\log(L_{\rm B}/L_\odot)$ | | 3.474±0.047 |
| Distance ($d$, pc) | | 987±17 |

## 3 IMPROVED ANALYSIS OF THE BINARITY

### 3.1 Spectral disentangling

We applied the technique of spectral disentangling (SPD) in velocity (Fourier) space as implemented in the FDBINARY code (Ilijić et al. 2004), using three spectral intervals centred on strong helium or metal lines (He I 4471 Å and Mg II 4481 Å; He I 4920 Å; the Si III triplet at 4550–4575 Å). The orbital elements we deduced are the time of periastron, $T_{\rm peri}$, the eccentricity, $e$, the longitude of periastron, $\omega$, and the amplitudes of the RV variations for the primary (star A) and secondary (star B) components, $K_{\rm A}$ and $K_{\rm B}$.

Since the effective temperatures ($T_{\rm eff}$) of the two stars are similar (Guinan et al. 2000; Pavlovski et al. 2009), their spectra are also similar at optical wavelengths. The orbital solutions for all three considered short spectral intervals led to a consistent set of values: $T_{\rm peri} = 54602.824 \pm 0.161$ d, $e = 0.2338 \pm 0.0026$, $\omega = 139.54 \pm 0.58$ degrees, $K_{\rm A} = 94.266 \pm 0.034$ km s$^{-1}$ and $K_{\rm B} = 154.59 \pm 0.31$ km s$^{-1}$. The quoted errors are the standard deviations of the SPD solutions for the three selected wavelength ranges.

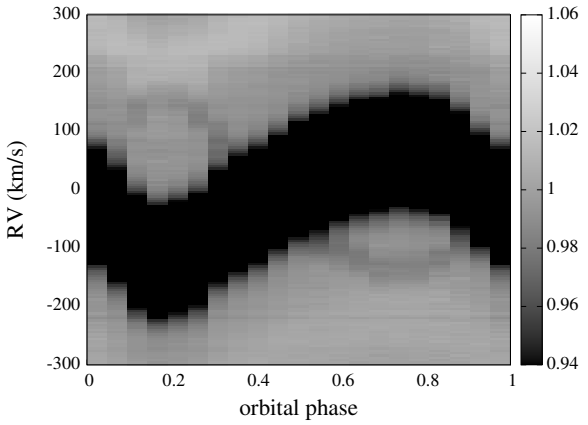


**Figure 2.** Gray-scale representation of the LSD profiles folded according to the orbital period of 12.425719 d. Phase zero corresponds to the time of primary minimum as derived by Guinan et al. (2000).

### 3.2 Light curve modelling

The orbital effects in the light curves were modelled using the Wilson-Devinney code (Wilson & Devinney 1971) in its 2004 version (hereafter WD2004), with automatic iteration performed using the JKTWD wrapper (Southworth et al. 2011). We converted the data to orbital phase using the ephemeris of Guinan et al. (2000), sorted them and reduced them into 202 binned datapoints. The bins cover the eclipses five times finer than other phases, but are otherwise equally spaced.

A variety of possible solutions were tried, with different numbers of fitted parameters and model options. The full set of input, output and control quantities for our final solution is given in Table 1 and the fit is shown as a full line in the upper panel of Fig. 1. The fit was performed in Mode 0, which renders the effective temperatures inconsequential by decoupling them from the solution. The detailed treatment of reflection was found to be necessary for V380 Cyg. We assumed gravity darkening coefficients and albedos of unity. Third light was found to be negligible so was set to zero. A linear limb darkening law was used, and bolometric coefficients for both stars plus the $K_{\rm p}$-band coefficient for star B were fixed to values obtained using the tables of Van Hamme (1993). The uncertainties on the photometric parameters listed in Table 1 come from the scatter of appropriate solutions with different sets of fitted parameters, and are much greater than the formal errors of the best single solution.

For our adopted solution we fitted for a phase shift with respect to the orbital ephemeris, the potentials and $K_{\rm p}$-band light contributions of the two stars, the $K_{\rm p}$-band limb darkening coefficient of the primary star (star A), $e$, $\omega$ and the orbital inclination. These parameters are given in the lower part of Table 1 alongside uncertainty values obtained by comparing all preliminary solutions providing a good fit with physically reasonable parameter values. We also give the fractional radii (stellar radii divided by the orbital

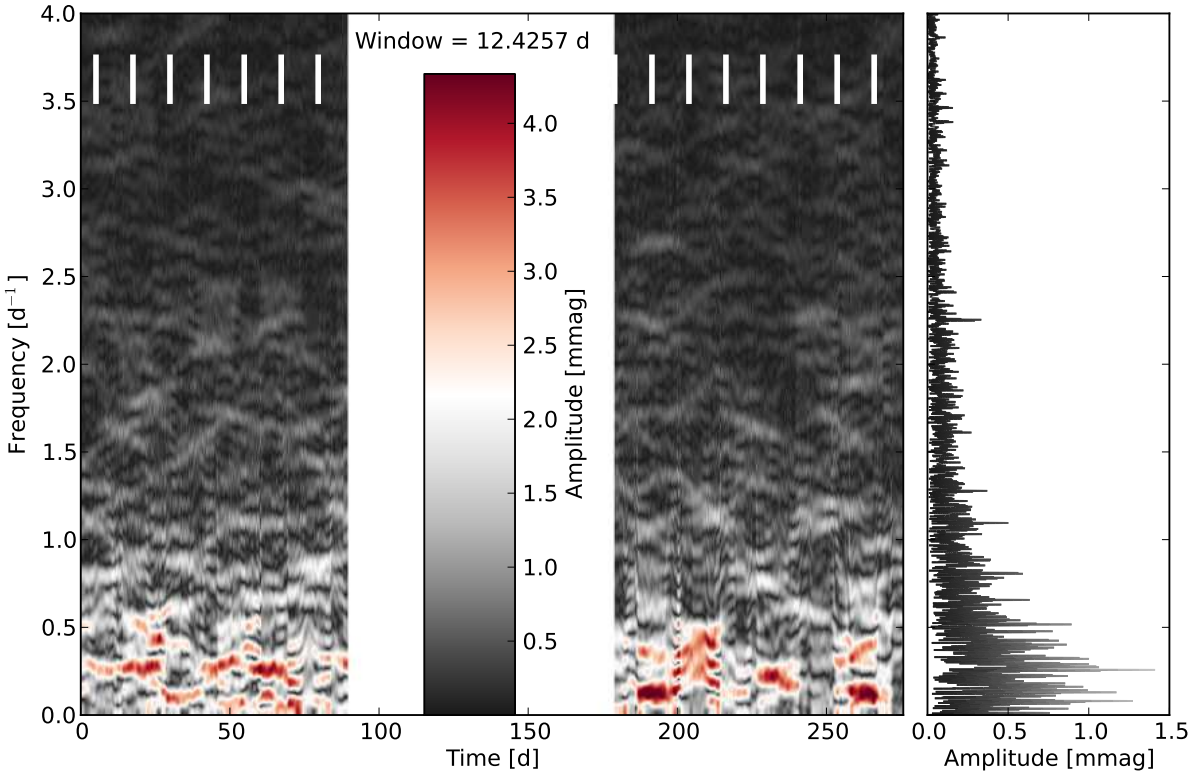


**Figure 3.** Left: Short Time Fourier Transform of the residual light curve shown in the middle panel of Fig. 1, for a window width of $P_{\rm orb}$. Right: summed amplitude spectrum. Thick white lines near the top of panels indicate the position of periastron passages.

semimajor axis) which are needed to calculate the physical properties of the two stars. There is a good agreement with the parameters found by Pavlovski et al. (2009). Table 1 also contains the full physical properties of the V380 Cyg system, calculated using the ABSDIM code (Southworth et al. 2005), our new spectroscopic and photometric results, and the $T_{\rm eff}$ values found by Pavlovski et al. (2009). For distance we quote the value obtained using the 2MASS $K_s$ apparent magnitude, bolometric corrections from Bessell et al. (1998), and adopting a reddening of $E(B-V) = 0.21 \pm 0.03$ mag.

We estimated the projected rotational velocity of V380 CygA from a spectrum taken at periastron and one at apastron, taking into account rotational and thermal broadening but ignoring pulsational broadening — see Sect. 4. The values are $91.5\pm7.0\,{\rm km\,s^{-1}}$ and $96.5\pm7.0\,{\rm km\,s^{-1}}$, respectively, and point to a higher rotation rate at apastron than at periastron, although the two values are within their error bars. In any case, none of the two values is compatible with synchronous rotation, which would require $66.1\pm1.1\,{\rm km\,s^{-1}}$ for the radius we found. Assuming the rotational axis to be perpendicular to the orbital plane, not necessarily the case in an eccentric non-synchronised binary, we estimate $f_{\rm rot}$ to be $0.115\,{\rm d^{-1}}$ at periastron and $0.121\,{\rm d^{-1}}$ at apastron.

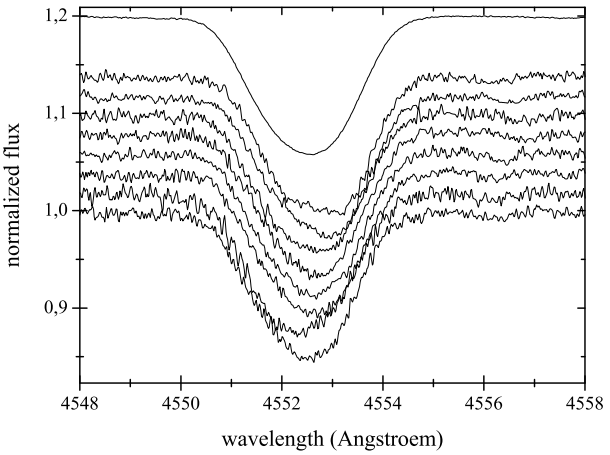


**Figure 4.** Snapshots of the Si III line and its disentangled version for star A shifted to its center of gravity after subtraction of the disentangled profile of the secondary.

## 4 THE INTRINSIC VARIABILITY OF THE PRIMARY

The residuals of the light curve of both Q7 and Q9 (see middle panel of Fig. 1 for Q9) were subjected to frequency analysis after detrending. The outcome in the region $[0,4]\,{\rm d^{-1}}$ ($[0,46]\,\mu$Hz) is shown in the right panel of Fig. 3. Strong excess power is present at numerous frequencies below $1\,{\rm d^{-1}}$ ($11.57\,\mu$Hz), the highest amplitude signals being very significant — see Table 4, where the significance level was computed from the local average amplitude in the spectrum over a range of $3\,{\rm d^{-1}}$. In addition, isolated peaks occur in $[1,4]\,{\rm d^{-1}}$. Most of the significant frequencies are multiples of the orbital frequency, while others are not. The Short Term Fourier Transform computed for a window width taken equal to the orbital period (left panel of Fig. 3) shows that part of the variability damps and re-appears throughout the data set.

We also searched for residual variability in the strong Si III line of the primary after SPD (Fig. 4). We computed the line moments

**Table 2.** Results of the frequency analysis from the various diagnostics after orbital subtraction. The Rayleigh limit amounts to $0.0036\,\mathrm{d}^{-1}$ for the photometry and $0.0071\,\mathrm{d}^{-1}$ for the spectroscopy.

| Diagnostic | Frequency ($\mathrm{d}^{-1}$) | Factor $f_{\rm orb}$ | Amplitude | Significance level (S/N) |
|---|---|---|---|---|
| *Kepler* LC | 0.2572 | 3.20 | 1.40 | 8.0 |
| (mmag) | 0.0802 | 1.00 | 1.25 | 7.1 |
| | 0.1295 | 1.61 | 1.15 | 6.6 |
| | 0.2769 | 3.44 | 1.02 | 5.8 |
| | 0.3204 | 3.98 | 1.00 | 5.7 |
| | 0.1611 | 2.00 | 0.98 | 5.6 |
| | ⋮ | ⋮ | ⋮ | ⋮ |
| | 3.4611 | 43.01 | 0.16 | 3.6 |
| | 3.3802 | 42.00 | 0.16 | 3.5 |
| | 2.2535 | 28.00 | 0.31 | 3.5 |
| | 0.8053 | 10.01 | 0.56 | 3.2 |
| $< v >$ | 0.0800 | 0.99 | 1.64 | 8.5 |
| ($\mathrm{km\,s}^{-1}$) | 0.8062 | 10.02 | 1.17 | 6.1 |
| | 0.8853 | 11.00 | 0.94 | 4.9 |
| | 0.2738 | 3.40 | 0.80 | 4.2 |
| | 1.3682 | 17.00 | 0.57 | 3.0 |
| Pixel-by-pixel | 0.8868 | 11.02 | 0.0104 | 5.2 |
| (continuum units) | 0.0350 | 0.43 | 0.0118 | 3.8 |
| | 0.0797 | 0.99 | 0.0099 | 3.2 |

following the definition of Aerts et al. (2010) of all 406 spectra, corrected for the disentangled profile of the secondary and shifted to the center of gravity of the primary. The $\langle v \rangle$-values obtained in this way for the spectra taken simultaneously with the *Kepler* Q9 photometry are shown in the lower panel of Fig. 1 while the frequencies found in this independent data set are also listed in Table 4. A pixel-by-pixel analysis (Zima 2008) was also done. Comparing all frequency analyses results in Table 4 leads to the conclusion that the line-profile variability of the primary is compatible with the *Kepler* residual photometry in the sense that power is found at multiples of $f_{\rm orb}$ and at some other frequencies. The frequencies in the disentangled Si III lines cannot be due to the prewhitening of the orbital motion, because the variability occurs as *asymmetries* in the profiles and are thus intrinsic to the primary (Fig. 4).

## 5 DISCUSSION AND INTERPRETATION

The intrinsic photometric and line-profile variability detected in the residual data of V380 Cyg A after orbital subtraction are naturally explained in terms of gravity-mode oscillations. Other causes of the intrinsic variability, such as migrating spots or rotational modulation, are unlikely as they would require a complex time-varying surface pattern and one would expect a much more prominent presence of the rotational frequency in that case. We also found no evidence of mass loss in the spectroscopy.

Some of the intrinsic frequencies detected in V380 Cyg A are connected with the orbital frequency. Given their time-dependent amplitudes (Fig. 3) we suspect that they are tidally triggered at periastron while damped further in the orbit. If confirmed, this finding holds the potential to model the interior structure of the primary in great detail and to deduce a seismic estimate of the core overshooting parameter which can then be compared with the one deduced from isochrone fitting. However, additional data are needed to deduce if the amplitude and frequency behaviour is indeed repetitive for numerous orbits. Such a situation was found for few close binaries so far. One case is HD 174884, an eccentric short-period binary consisting of two cool B stars with residual variability at low-order multiples of the orbital frequency and two tidal oscillations induced at 8 and 13 $f_{\rm orb}$ (Maceroni et al. 2009). Resonant mode locking at 90 and 91 $f_{\rm orb}$ occurs in the highly eccentric 42 d binary HD 187091 consisting of two A stars (KOI-54, Welsh et al. 2011). In contrast to these two cases, V380 CygA exhibits an excess bump of power rather than only well-isolated stable frequencies. Future *Kepler* data will cover three more quarters while additional spectroscopy will be gathered to unravel the pulsational behaviour of this massive binary.

## ACKNOWLEDGEMENTS

Funding for the *Kepler* Discovery mission is provided by NASA's Science Mission Directorate. The authors gratefully acknowledge the *Kepler* and Mercator teams, whose outstanding efforts have made these results possible, and Dr. Yves Frémat for carrying out part of the observations with the Mercator telescope. The research leading to these results has received funding from the European Research Council under the European Community's Seventh Framework Programme (FP7/2007–2013)/ERC grant agreement n°227224 (PROSPERITY). JS acknowledges financial support from STFC in the form of an Advanced Fellowship. PD and BD are Postdoctoral and Aspirant Fellow of the FWO, respectively. JD is funded by the Belgian federal science policy office Belspo. PN is Boursier F.R.I.A., Belgium.

## REFERENCES

Aerts, C., Christensen-Dalsgaard, J., & Kurtz, D. W. 2010, Asteroseismology, Springer, Heidelberg
Aerts, C., et al. 2003, Sci, 300, 1926
Aerts, C., et al. 2011, A&A, 534, A98
Bessell, M., Castelli, F., & Plez, B. 1998, A&A, 333, 231
Briquet, M., et al. 2007, MNRAS, 381, 1482
Briquet, M., et al. 2011, A&A, 527, A112
Bryson, S. T., et al. 2010, ApJ, 713, L97
Donati, J.-F., et al., 1997, MNRAS, 291, 658
Guinan, E., et al. 2000, ApJ, 544, 409
Ilijić, S., et al. 2004, ASPC, 318, 111
Kolenberg, K., et al. 2011, MNRAS, 411, 878
Maceroni, C., et al. 2009, A&A, 508, 1375
Pamyatnykh, A. A., Handler, G., & Dziembowski, W. A. 2004, MNRAS, 350, 1022
Pavlovski, K., et al. 2009, MNRAS, 400, 791
Popper, D. & Guinan, E. F. 1998, PASP, 110, 572
Raskin, G., et al. 2011, A&A, 526, A69
Southworth, J., Maxted, P. F. L., Smalley, B. 2005, A&A, 429, 645
Southworth, J., et al. 2011, MNRAS, 414, 2413
Van Hamme, W. 1993, AJ, 106, 2096
Wilson, R. E., & Devinney, E. J. 1971, ApJ, 166, 605
Wilson, R. E., & Van Hamme, W. 2004, Computing Binary Star Observables (Wilson-Devinney program user guide), Univ. of Florida, Gainsville
Welsh, W. F., et al. 2011, ApJS, 197, 4
Zima, W. 2008, CoAst, 155, 17